This is a “preproof” accepted article for *Clay Minerals*.
This version may be subject to change during the production process.
10.1180/clm.2025.4

Thermo-physical and Viscoelastic Peculiarities of 3,4-Dihydro-2H-pyran Containing Polymer Layered-Clay Reinforced Nanoarchitectures

Burcu Akar, Özlem Şahin, Hatice Kaplan Can*

Hacettepe University, Faculty of Science, Division of Polymer Chemistry,

06800, Beytepe, Ankara, Türkiye

Corresponding author: hkaplan@hacettepe.edu.tr

ABSTRACT

This study focuses on the synthesis of poly(3,4-dihydro-2H-pyran-*alt*-maleic anhydride) [poly(DHP-*alt*-MA)] and poly(3,4-dihydro-2H-pyran-*co*-maleic anhydride-*co*-vinyl acetate) [poly(DHP-*co*-MA-*co*-VA)] their nanocomposites modified with organoammonium salts. The goal was to investigate the structural, dynamic mechanical and thermal properties of polymers and nanocomposites with particular emphasis on the role of the organoclay modification. In this study, bentonite was modified using alkyl ammonium salts with varying

https://doi.org/10.1180/clm.2025.4 Published online by Cambridge University Press

chain lengths (C14, C16, and C18). Ion exchange processes led to the transformation of bentonite from a hydrophilic to a hydrophobic character, facilitating the formation of hybrid structures. Dynamic mechanical analysis (DMA), differential thermal analysis (DTA), differential scanning calorimetry (DSC), and thermogravimetric analysis (TGA) were used to characterize the viscoelastic and thermal properties of the polymers and their nanocomposites. The results showed that the incorporation of organoclay structures, particularly those modified with C18 alkyl groups significantly enhanced the viscoelastic properties with the highest storage modulus observed in the nanocomposites. The thermal analysis revealed that the nanocomposites exhibited a distinct three-step degradation process, unlike the copolymer, which underwent two-step degradation. Despite this difference, no significant improvement in thermal stability was observed in the nanocomposites compared to the copolymers. The study concludes that the incorporation of long-chain alkyl ammonium salts into bentonite and their use in copolymerization significantly impacts the thermal and dynamic mechanical properties of the resulting nanocomposites. The modification of bentonite with C18 alkyl groups led to the most stable and dynamic mechanically robust nanocomposites, providing valuable insight into the role of organoclay modification in enhancing the performance of polymer-based nanocomposites.

Keywords: Nanocomposite, Bentonite, Poly(DHP-*alt*-MA), Poly(DHP-*co*-MA-*co*-VA), DMA

INTRODUCTION

The integration of materials science and nanotechnology has given rise to the field of nanocomposites, characterized by at least one nanoscale dimension within the phases involved. Since their inception around 1990, polymer nanocomposites (PNCs) composed of nanoparticles in the form of spheres, rods, or plates have captured considerable interest from both academia and industry.(Okamoto & Ray, 2004) These "materials of the new century" are celebrated for their exceptional properties, which enable a wide array of innovative applications.(Ray & Okamoto, 2003) Nanocomposites enhance polymers with diverse thermal and functional properties.(Kaplan Can & Şahin, 2015) While PNCs have gained substantial recognition for their enhanced properties, the challenge remains in

https://doi.org/10.1180/clm.2025.4 Published online by Cambridge University Press

effectively integrating these materials with functional polymers to optimize their potential.(Liang *et al.*, 2021)

Organically modified layered silicates, or nanoclays, are extensively utilized in various fields including coatings, cosmetics, drug delivery, and gas adsorption.(Okada & Usuki, 2006) The functional properties of copolymers and terpolymers can be finely tuned by selecting appropriate mole percentages and integrating these nanoclays, which typically involve at least two distinct monomers.(Kelley *et al.*, 2013; Murugesan & Scheibel, 2020) With approximately thirty types of nanoclays available, each tailored for specific applications due to its unique mineralogical composition (Mobaraki *et al.*, 2022), their potential in biomedical applications is significant. Research has explored their use in chemotherapy, scaffold design, bone adhesion, wound healing, drug delivery, tissue reconstruction, and enzyme immobilization.(Rawtani & Agrawal, 2012; Mortimer *et al.*, 2016; Wu *et al.*, 2017)

However, while there is growing interest in these materials, there is a clear gap in understanding how the inclusion of specific types of nanoclays, particularly bentonite, can lead to more efficient drug delivery systems and other biomedical innovations.(Mir *et al.*, 2025) The advancement of material technology has opened new avenues for polymer-nanoclay composites, which offer high density, strength, large surface areas, elasticity, and enhanced fire resistance, along with remarkable thermomechanical, optoelectronic, and magnetic properties.(Nazir *et al.*, 2016) These properties enable the development of high-performance composites that significantly outperform traditional materials. Polymer-clay nanocomposites, featuring clay particles smaller than nanometers, exhibit high hardness and barrier resistance.(Van Es, 2001) The diverse applications of clays are attributed to their biocompatibility, environmental friendliness, affordability, and versatility.(Müller *et al.*, 2017) Despite these promising features, the mechanisms through which these clays interact with the organic matrices at the molecular level remain underexplored, limiting their broader industrial and biomedical application. Clays are particularly favored for biomedical applications due to their safety and ecological benefits.(Li *et al.*, 2010; Vergaro *et al.*, 2010; Sánchez-Fernández *et al.*, 2014) Historically, clays have been studied for their ability to combat infections, reduce diarrhea and inflammation, purify blood, and heal ulcers.(Ranjan *et al.*, 2025)

https://doi.org/10.1180/clm.2025.4 Published online by Cambridge University Press

Their notable attributes include high permeability, specific surface characteristics, low density, extensive surface coverage, and excellent biological compatibility.(Williams & Haydel, 2010; Singh *et al.*, 2015) However, the specific biocompatibility and interaction of bentonite with various drugs and therapeutic agents remain an area where further studies are needed to fully realize its potential.(Wirtu *et al.*, 2025)

Among the various types of clays, natural bentonite, with its unique mineral composition and specific physicochemical properties, stands out as a material of particular interest in many applications. While many studies have focused on the general properties of bentonite, the incorporation of modified bentonite in polymer matrices to create nanocomposites is still a relatively underexplored field. Natural bentonite primarily forms through the weathering or hydrothermal alteration of volcanic ash in sedimentary environments, particularly under alkaline conditions. This alteration process results in the formation of bentonite deposits, which are commonly found in regions with significant volcanic activity, such as marine basins, lakes, or areas with long-standing hydrothermal systems. Bentonites are predominantly composed of montmorillonite, a 2:1 layered aluminosilicate mineral, which imparts swelling properties and a high cation-exchange capacity to bentonite.(Borah *et al.*, 2022)

In addition to its primary mineral, bentonites may also contain accessory minerals such as quartz, feldspar, kaolinite, illite, and calcite. These minerals contribute to the swelling behavior and high cation-exchange capacity characteristic of bentonite, which are essential for its diverse applications. The presence of these minerals also influences the physical properties of the clay. For instance, quartz or feldspar can reduce expansion, while kaolinite or illite can impact cation-exchange capacity and chemical reactivity. The mineralogical composition thus plays a crucial role in determining the suitability of bentonite for various applications.(Grim & Guven, 2011)

The ability of bentonite to undergo ion-exchange reactions is particularly important for enhancing its compatibility with organic matrices. Ion-exchange processes involve the substitution of small molecular cations (e.g., Na^{+} or Ca^{2+}) with larger organic cations, which improves the dispersion of bentonite in polymer matrices and facilitates the formation of nanocomposites. These ion-exchange processes enhance the potential of bentonite to be utilized not only in drug delivery but also in environmental and pharmaceutical applications, thus increasing the versatility of this material.(Marouf *et al.*, 2021)

https://doi.org/10.1180/clm.2025.4 Published online by Cambridge University Press

Bentonite's physicochemical properties, such as swelling behavior, cation-exchange capacity, and thermal stability, are directly influenced by its mineralogical composition. The 2:1 layered structure enables bentonite to absorb water and swell, making it ideal for applications requiring high viscosity or water retention. Its cation-exchange properties allow bentonite to adsorb and exchange ions, while the presence of minerals like quartz improves its thermal stability.(Borah *et al.*, 2022)

A detailed understanding of bentonite's mineralogical composition and physicochemical properties is essential for optimizing its use in various industrial, pharmaceutical, and environmental applications. This understanding allows for the development of specific functional materials that cater to the demands of next-generation drug delivery systems.

Bentonite can not only inhibit the growth of cancer cells (Sabzevari *et al.*, 2024), but also can be used as a carrier for imaging/therapeutic agents in theranostic anticancer products (Chan *et al.*, 2021). Due to its excellent biocompatibility, bentonite is widely used for oral (Sabzevari & Sabahi, 2022) and ocular (Zhao *et al.*, 2024) delivery of drugs. This further underscores bentonite's unique role as a promising material for controlled drug release, providing a foundation for novel therapeutic strategies.

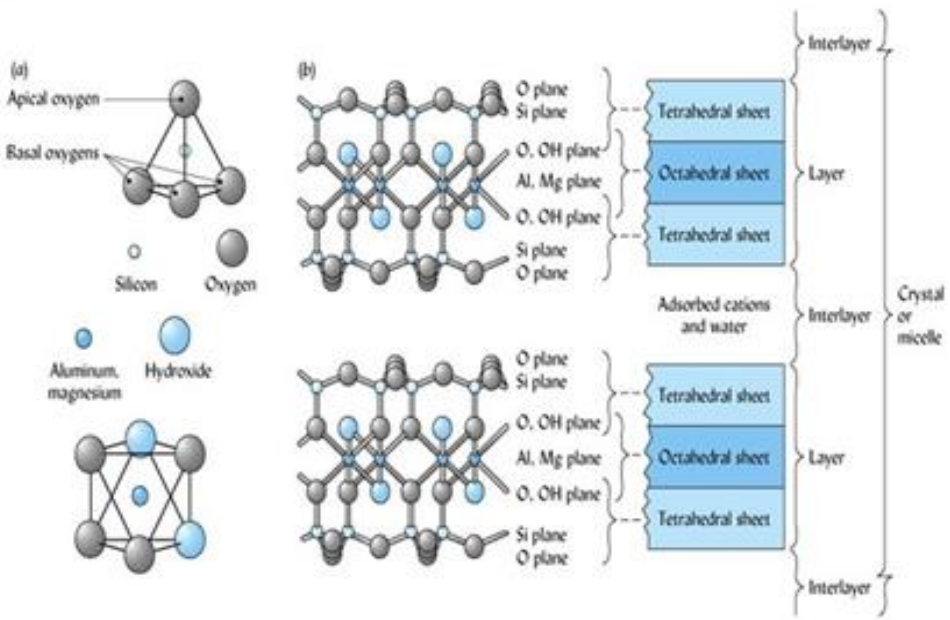

Scheme 1. Structure of bentonite clay. (Masindi, 2015)

Bentonite's has long been used as a binder, emulsifier, suspending agent, and viscosity modifier in pharmaceuticals.(Murray, 2006; Modabberi *et al.*, 2015) The clay characterized by

https://doi.org/10.1180/clm.2025.4 Published online by Cambridge University Press

its 2:1 layer structure of tetrahedral and octahedral sheets, plays a crucial role in determining the chemical and physical properties of bentonite.(Srasra *et al.*, 1989) The effectiveness of bentonite in pharmaceuticals is closely linked to its primary component which features a 2:1 layer structure crucial for its chemical and physical properties. However, the interaction between untreated clay and organic matrices is limited, posing challenges for the creation of nanocomposites. To overcome this, ion exchange processes are employed to modify the clay's surface by substituting small molecular cations with organic cations, thereby improving compatibility with various polymer matrices.

Creating nanocomposites from untreated clay is challenging due to the lack of interaction between untreated clay and the organic matrix. To address this, ion exchange is employed to modify the clay's surface, substituting small molecular cations with organic cations to enhance compatibility with various matrix polymers.(Lan & Pinnavaia, 1994) Water-soluble copolymers containing anhydrides, known as polyanions and their derivatives, exhibit significant physiological and biological effects, including antibacterial and anticancer properties, immune system stimulation, and enhanced resistance to tumors, viruses, and bacteria.(Donaruma *et al.*, 1980; OTTENBRITE, 1982; Gorshkova & Stotskaya, 1998)

In this study, charge transfer complex (CTC) polymerization was used to synthesize co- and terpolymers of polymer/clay nanocomposites. This study addresses a critical gap in the literature by using modified nanoclays and comparing their properties in the context of thermally stable and bioactive nanocomposites for drug carrier systems. The research focuses on producing modified nanoclays using three different alkyl ammonium salts, which are then employed in synthesizing poly(3,4-Dihydro-2H-pyran-*alt*-maleic anhydride) (poly(DHP-*alt*-MA)) and poly(3,4-Dihydro-2H-pyran-*co*-maleic anhydride-*co*-vinyl acetate) [poly(DHP-*co*-MA-*co*-VA)] nanocomposites.(Can *et al.*, 2022) Previous studies have examined copolymers of poly(DHP-*alt*-MA) and related nanocomposites, as well as terpolymer/organically modified bentonite nanocomposites due to the their anticancer and antitumor activity potential properties (Can *et al.*, 2005; Can *et al.*, 2022) In this study compares thermal characteristics, stability, and viscoelastic properties of these nanocomposites, exploring structural changes induced by the incorporation of three distinct alkyl ammonium salts In order to elucidate the characteristics that have not been studied before in the literature.

https://doi.org/10.1180/clm.2025.4 Published online by Cambridge University Press

EXPERIMENTAL

Materials

Initial monomer 3,4-Dihydro-2H-pyran (DHP) supplied by Sigma-Aldrich was distilled before use. Maleic Anhydride (MA: m.p 52,8 °C; Fluka) was purified before use by recrystallization from anhydrous benzene and sublimation in a vacuum. Vinyl acetate was supplied from Aldrich. 2,2-Azobisisobutyronitrile (AIBN; Fluka), used as an initiator, was twice recrystallized from a chloroform solution by methanol. Bentonite was supplied by CAS number 1302-78-9 Sigma-Aldrich as hydrophilic bentonite nanoclay. The organo-bentonite was prepared by with octadecyltrimetilammonium bromide (ODTMAB) (Fluka), hexadecyltrimetilammonium bromide (HDTMAB) (Sigma-Aldrich) and tetradecyl (trimethyl) ammonium bromide (TDTMAB) (Sigma-Aldrich). Other reagents, including organic solvents, were purified by ordinary methods.

Organophilic Modification of Bentonite

Through a cation-exchange reaction with octadecyltrimethyl ammonium bromide (ODTMAB), hexadecyltrimethyl ammonium bromide (HDTMAB), and tetradecyl(trimethyl)ammonium bromide (TDTMAB) (Scheme 2), natural bentonite underwent modification to yield organophilic clay. This process, documented in previous research, elucidates the modification of bentonite.(Can *et al.*, 2022)

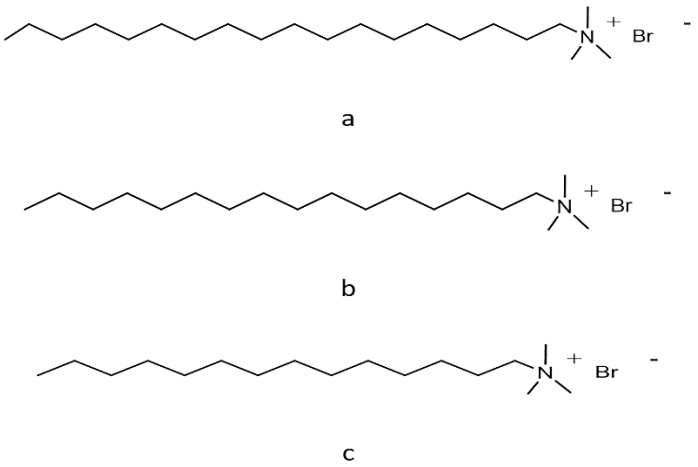

Scheme 2. Chemical structure of **a)** octadecyltrimethyl ammonium bromide (ODTMAB), **b)** hexadecyl-trimethyl ammonium bromide (HDTMAB), and **c)** tetradecyl (trimethyl) ammonium bromide (TDTMAB) salts.(Can *et al.*, 2022)

https://doi.org/10.1180/clm.2025.4 Published online by Cambridge University Press

Polymer Synthesis: Copolymer and Terpolymer Procedures

Monomers including 3,4-dihydro-2H-pyran (DHP), maleic anhydride (MA), and vinyl acetate (VA) were utilized in the polymerization processes. Radical solution polymerization was conducted, employing a charge transfer complex formation with electron acceptor and donor monomer systems (Scheme 3). The monomer ratios by weight were set at 50% for DHP: MA and 25% for each DHP:MA: VA (Scheme 4). As a preliminary stage of polymerization; DHP, MA, and VA monomers were dissolved in methyl ethyl ketone (MEK) solvent at a ratio of 70% (monomer/solvent), with AIBN used as the initiator (0.5% by weight of total monomers). In glass tubes, the copolymerization and terpolymerization procedures were carried out, dissolving the monomers and initiator (AIBN) in methyl ethyl ketone (MEK) for 9 hours at 75 °C under a nitrogen atmosphere, employing a constant temperature glycerin bath. After this duration, the copolymer, existing in a homogeneous phase, was precipitated in diethyl ether, while the terpolymer was precipitated in n-hexane within an ice bath. The purified polymers underwent rinsing in diethyl ether and were dried under vacuum at 40 °C until reaching a constant weight.

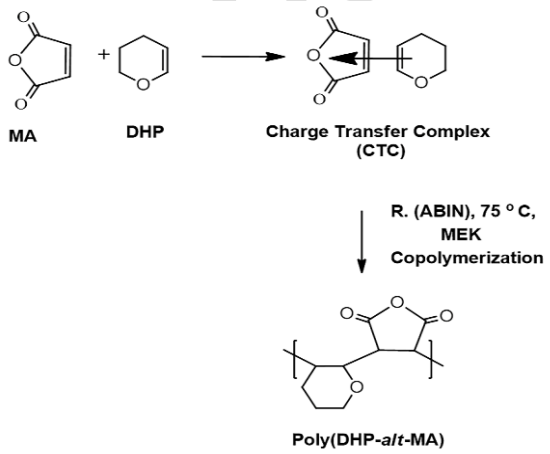

Scheme 3. Schematic representation of the synthesis of alternating copolymer *via* charge transfer complex (CTC) method (Can *et* al., 2022)

Preparation of polymer–clay nanocomposites (PCN's)

Copolymer/clay and terpolymer/clay nanocomposites (PCN's) were prepared in the same composition as copolymer and terpolymer by using organically modified clay and starting monomers feed. Organo-bentonites prepared with alkyl ammonium salts were used at the rate of 5.0% of the total mass of clay, monomers and the initiator.

https://doi.org/10.1180/clm.2025.4 Published online by Cambridge University Press

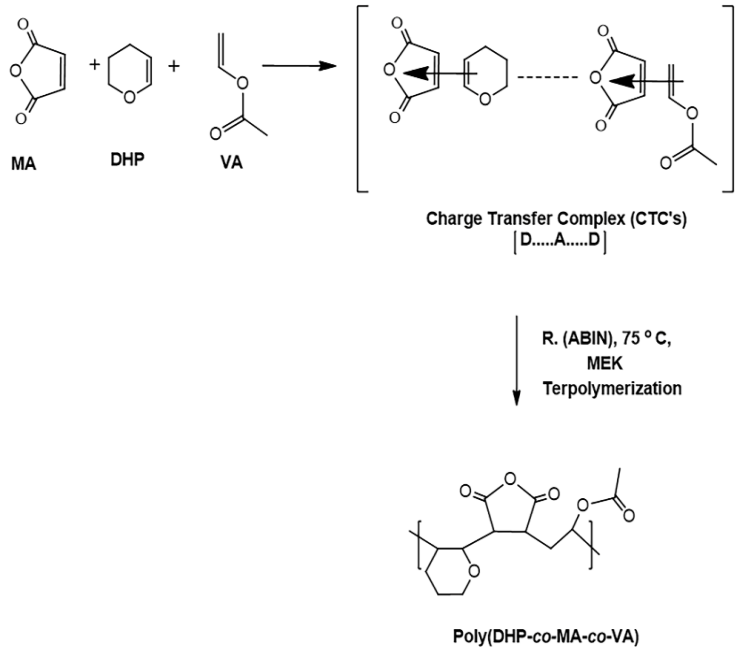

Scheme 4. Preparation pathway of terpolymerization of 3,4-Dihydro-2H-pyran (DHP),maleic anhydride (MA), and vinyl acetate (VA) monomers *via* charge transfer complex (CTC).(Can *et al.*, 2022)

Organo-bentonites were suspended in 15 mL of MEK at room temperature in a glycerin bath for 1 hour. By adding monomers, organo-clay were mixed and mixed for 3 hours to form a suspension. Following a 3-hour mixing period, the initiator and residual solvent were introduced, and the reaction proceeded for an additional 9 hours at 75 °C under a nitrogen atmosphere within the tubes. The copolymer-clay nanocomposites were precipitated in diethyl ether in an ice bath, while the terpolymer-clay nanocomposites were precipitated in n-hexane in an ice bath. The filtered nanocomposites were subsequently dried under vacuum at 40 °C until a constant weight was achieved.

Thermogravimetric Analysis (TGA), Differential Thermal Analysis (DTA) and Differential Scanning Calorimetry (DSC) Measurements

To investigate the structural and thermal properties of poly(DHP-*alt*-MA) copolymer, poly(DHP-*co*-MA-*co*-VA) terpolymer, and nanocomposites derived from these structures, TGA, DTA, and DSC analyses were conducted; Samples were analyzed using a Shimadzu DTG 60 H instrument at a flow rate of 10 mL/min, at a sample weight of 2-5 mg in nitrogen environment.

https://doi.org/10.1180/clm.2025.4 Published online by Cambridge University Press

Dynamic Mechanical Analysis Measurements

Dynamic mechanical behaviors of copolymers and nanocomposites were performed with TA Q800 Dynamic Mechanical Analyzer. Mixtures of polymers and nanocomposites with Al_2O_3 (50:50 wt%) were prepared and these powdered mixtures were loaded onto DMA using a dust trap. DMA curves were taken at a constant frequency (ω= 1 Hz) over the temperature range of 20 °C to 200 °C and 3 °C/min temperature scanning range.

RESULTS AND DISCUSSION

Thermal Analysis of Organophilic Modification Bentonite

Thermal analysis of organophilic modification of bentonite *via* organoammonium salts was followed by TGA. Figures 1 and 2 display the composition of three distinct organoammonium-modified bentonites, as well as the TGA and first derivative (DTG) of the TGA curve of bentonite. At 100 °C, pristine bentonite (Figures 1-a and 2-a) revealed a 13% mass loss. This phenomenon might be interpreted as the loss of the structure-attached H_2O from the bentonite structure. And also after modification, the transformation of Na+ Bentonite from hydrophilic to hydrophobic was seen. It displays a one-step degradation when taking into account the temperature-dependent mass loss of bentonite (TGA, Figure 1-a). 80% of the pristine bentonite, which represents its ultimate thermal stability, is shielded from a breakdown between 100 and 600 °C. The transfer of heat is efficiently inhibited by bentonite, an inorganic material that is well-known for its strong thermal stability and formidable barrier qualities. Moreover, the TGA and DTG diagrams of bentonites modified with long aliphatic chains, including C14, C16, and C18, show different cascade degradation behaviors in comparison to the behavior shown in materials of bentonite. In contrast to bentonite mass loss-temperature curves, organo-bentonite complexes exhibit two-step degradation. At 100 °C, the first degradation is the loss of water. In all organo-bentonite structures, the most significant degradation occurs between 280 and 300 °C. The decomposition of long aliphatic chains in bentonite from changed organoammonium salts might account for this significant degradation peak.

https://doi.org/10.1180/clm.2025.4 Published online by Cambridge University Press

Table 1. Thermoanalytical results of bentonite, TDTMAB-modified bentonite, HDTMAB-modified bentonite and ODTMAB-modified bentonite: % mass loss of clays at certain temperatures

	Mass Loss (%)-Temperature (°C)					
Clays	**100 °C**	**200 °C**	**300 °C**	**400 °C**	**500 °C**	**600 °C**
Bentonite	13.07	1.06	1.01	1.83	2.13	3.43
TDTMAB-modified bentonite	3.62	1.03	9.48	9.22	8.34	1.79
HDTMAB-modified bentonite	3.41	0.88	13.73	8.95	5.56	1.78
ODTMAB-modified bentonite	2.32	1.30	14.72	11.92	7.85	1.72

(TDTMAB: tetradecyl (trimethyl) ammonium bromide; HDTMAB: hexadecyltrimethyl ammonium bromide; ODTMAB: octadecyltrimethyl ammonium bromide)

Table 1 shows that the percentage of weight decrease detected in the HDTMAB and ODTMAB-modified bentonite is 13.73% and 14.72%, respectively. When examined at the DTG peaks, notice that the degradation stage in both the HDTMAB and ODTMAB-modified nanostructures was roughly close. This might be stated as follows: the structures' C16 and C18 chain lengths are closer to each other. Furthermore, the bentonite structure changed with TDTMAB (C14) and had a 9.48% mass reduction. In all modified bentonite structures, the change that occurs in step 2 is smaller.

The elimination of smaller structures from the compound can be the explanation for thermal decomposition peaks occurred around 400 and 500 °C. The thermogram of the highest degradation (Figure 1-b TGA) has been determined to correspond to the structure containing C18 chains modified with ODTMAB (39.3%) at about 600 °C. The bentonite treated with TDTMAB (33.48%) is the modified structure that had the least amount of heat degradation (Figure 1-d). The thermograms and mass loss percentage values show that ion exchange

https://doi.org/10.1180/clm.2025.4 Published online by Cambridge University Press

reactions can modify bentonite through the addition of aliphatic long-chain structures to ODTMAB, HDTMAB, and TDTMAB.

Dynamic Mechanical Analysis of Organophilic Modification Bentonite

Dynamic mechanical analysis (DMA) is an important method that provides deep insights into the behaviors and characteristics of materials. Designed especially for the complex analysis of polymers, DMA uses a sinusoidal stress application method to investigate the viscoelastic properties of materials. By accurately measuring strain in response to stress, DMA facilitates understanding of modulus, which defines stiffness and damping properties as storage modulus (SM) and loss modulus (LM), respectively. These metrics provide important insights into energy storage and dissipation mechanisms within the material matrix, as well as quantify the material's elastic and viscous responses. Figure 3 displays the storage modulus (SM) diagrams of organoclay compounds that have been changed with bentonite and alkyl ammonium groups of C14, C16, and C18, as shown in the DMA data. After analyzing the graphs shown in Figures 3-b, c, and d, it is evident that there are significant differences in the storage modulus. The different carbon numbers of the ammonium salts used in the modification process are responsible for these differences. Observations indicate that bentonite exhibits the maximum level of strength, with the organoclay modified with C18 ammonium salt displaying the strength value closest to that of bentonite (Figure 3-b). Upon examining the SM curves depicted in Figure 3, it is evident that there is minimal disparity resulting from alterations in the glassy zone, namely below 100 °C. However, the SM values exhibit a clear correlation with the length of the carbon chain in the glassy transition region (100–200 °C). Whereas a similar tendency is found in the ductile area between 200 and 300 °C, the SM values fall as the carbon number decreases as the alkyl groups enter the bentonite structure. Storage modulus values of layered silicate structures were separated and effectively changed with alkyl chains. Upon study of the LM-temperature curves illustrated in Figure 4 for both virgin and modified bentonite formations, considerable variations in the silica layers are observed, according to the length of the alkyl chains employed. The effective alteration of the inorganic bentonite structure with extended aliphatic groups leads to a proportionate rise in the LM value related to the number of carbon atoms in the chain.

https://doi.org/10.1180/clm.2025.4 Published online by Cambridge University Press

Tan δ, a crucial parameter determined from DMA curves, represents the ratio between the viscous and elastic moduli, providing a measure of damping inside a material. This ratio, indicative of the material's energy dissipation capabilities, gives insights into its efficiency in absorbing energy. Tan δ is defined below:

$$\text{Tan } \delta = LM/SM$$

In the alteration with the alkyl group containing C14 in Figure 5, two peaks are detected in the Tan δ curves (Figure 5-c), one of which diminishes upon modification with C16. When the alteration is done using C18 (Figure 5-b), just a single peak is detected. The single symmetrical peak maximum occurring in the center of the two maximum peaks found at C14 and C16 in the Tan δ-temperature curves demonstrates that C18 is the most suitable alteration.

Thermal Analysis of Poly(3,4-Dihydro-2H-pyran-*alt*-maleic anhydride) Copolymer and its Nanocomposites

Copolymers and nanocomposite structures obtained with three different organoammonium salt modifications were characterized using the thermal methods TGA, DTA, and DrDTA. Figure 6 shows the mass loss-temperature thermograms for the copolymer and modified nanocomposites. Upon analyzing the TGA thermogram presented in Figure 6-a for poly(DHP-*alt*-MA), it reveals a two-step degradation process, with the initial decomposition occurring at 250 °C, followed by a subsequent decomposition at 420 °C. Considering the 31.7% mass loss, the maximum degradation step at 420 °C from the DHP structure, which has groups that are more easily separated from the structure, can be interpreted as the degradation where species such as CO_2 are removed from the anhydrite ring (56.17% by weight). The predominant breakdown can be linked to the decomposition of the C-H linkages within the backbone of the polymer chain.

In contrast to the copolymer, the nanocomposites exhibit a distinct three-step degradation pattern in their thermal properties. Considering the mass loss-temperature thermograms up to 600 °C, it is the copolymer structure that has lost a lot of mass from nanocomposites. Upon examination of the thermoanalytical data for nanocomposites, it becomes evident that the initial step involves a loss of mass attributed to the evaporation of crystal water between

https://doi.org/10.1180/clm.2025.4 Published online by Cambridge University Press

100 and 150 °C, a phenomenon also observed in the pristine bentonite structure. Decomposition in the second step is the step in which the most mass loss is seen. The mass loss of modified nanostructures with ODTMAB, HDTMAB, and TDTMAB can be expressed as 36.93%, 50.66%, and 44.65%, respectively. 10% mass loss was observed in all 3 nanostructures similar to copolymers between 250 and 300 °C. The 3rd step of degradation is observed in nanostructures in the same way between 350 and 400 °C. By adding three different organoclay structures modified by copolymerization at 5.0%, nanostructures with similar thermal stability were obtained (Figures 6 and 7).

Table 2. Thermoanalytical results of Poly(DHP-*alt*-MA) and Poly(DHP-*alt*-MA)/organo-bentonite nanocomposites; %mass loss and T_g (^{0}C) values of copolymer and polymer/clay nanocomposites at certain temperatures

Samples	Glass Transition Temperatures T_g (°C)			Mass Loss (%)-Temperature (°C)					
	DTA	DSC	DMA	100	200	300	400	500	600
Poly(DHP-*alt*-MA)	133	131	118	2.10	21.30	34.85	56.20	87.40	89.10
Poly(DHP-*alt*-MA)/ODTMAB-bentonite nanocomposite	141	140	123	1.75	36.95	46.15	59.10	66.40	68.30
Poly(DHP-*alt*-MA)/HDTMAB-bentonite nanocomposite	140	135	133	2.00	50.65	59.95	72.40	79.80	81.45
Poly(DHP-*alt*-MA)/TDTMAB-bentonite nanocomposite	136	135	116	1.95	44.65	53.70	66.90	75.40	77.55

https://doi.org/10.1180/clm.2025.4 Published online by Cambridge University Press

(Poly(DHP-*alt*-MA): poly(3,4-dihydro-2H-pyran-*alt*-maleic anhydride); TDTMAB: tetradecyl (trimethyl) ammonium bromide; HDTMAB: hexadecyltrimethyl ammonium bromide; ODTMAB: octadecyltrimethyl ammonium bromide)

Table 2 displays the thermoanalytical data obtained using the DSC, DTA, and DMA (tan δ) curves. Glass transition temperature DTA (Figure 7), DSC, and DMA analyses are used comparatively. When the Tg values found by three different methods are compared and considered the C14-C18 chain lengths, there is a very good agreement between the Tg values obtained from DTA and DSC. The Tg values of the hybrid structures resulting from the incorporation of inorganic materials were found to be higher than those of the copolymer (132.7 °C).

The C16-C18 Tg values of nanocomposites modified with HDTMAB and ODTMAB were found to be very close to each other (140.56 °C and 140.78 °C). As a result of the characterization with thermal methods, it is observed that the nanostructures obtained by using inorganic-organic modified structures in the copolymerization environment gain thermal stability and carbon chain lengths play an important role in it. Among these methods, DMA was accepted as the most sensitive method used to determine Tg.

Dynamic Mechanical Analysis of Poly(3,4-Dihydro-2H-pyran-*alt*-maleic anhydride) Terpolymer and its Nanocomposites

The DMA parameters are utilized to offer valuable understanding regarding the even distribution of the organoclay structure in the polymer matrix. Looking at the storage modulus (SM)-temperature (T) curve (Figure 8), the copolymer clay nanocomposite structure constructed with the C18 alkyl group (Figure 8-a) displays the greatest storage modulus value. High storage modulus values are displayed by copolymer and polymer/clay nanocomposites in the glassy area of the SM-T curve, reaching temperatures of up to 60 °C. The sequential copolymer's storage modulus (SM) exhibits a significant decrease with increasing temperature, particularly in the 60–80 °C regions. However, it was shown that when the carbon chain length grew, the elastic modulus of the nanostructures made with modified clays C14, C16, and C18 rose as well. In storage modules graph, glassy transitions were observed in areas exhibiting elastic behavior. This indicates that the layered silicate structure is distributed throughout the polymer matrix.

https://doi.org/10.1180/clm.2025.4 Published online by Cambridge University Press

The graphs representing the loss modulus (Figure 9) and Tan δ (Figure 10) indicate the maximums at which Tg increases as temperature rises (Table 2). The fact that the damping is minimal below the glass transition and increases when the system reaches the Tg area of the glass transition shows that the "micro Brownian" motion between the molecular chains has started.(Ray & Okamoto, 2003) The scenario here may be explained by the fact that not all segments relax concurrently, while the glassy portions keep more energy. When it reaches the rubbery zone, the segments in the solid state become loose and release extra energy.

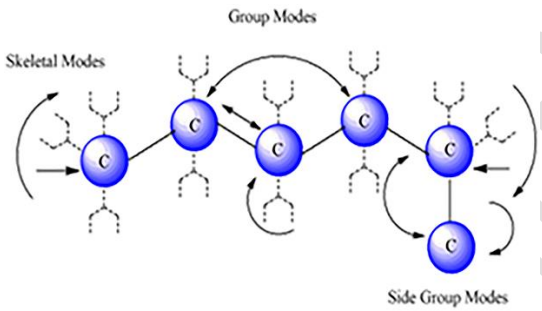

Scheme 6. Molecular modes of glass transition temperature (Tg)

The change of one chain of polymers to dispersion by connecting it to a different chain can be attributed to micro-Brownian action. The highest possible damping is seen where polymer chains are in contact with one another under harmonic stress. In this situation, the loss modulus drops beyond the glass transition, and near the glass transition, the segments tend to gain movement and resist flowing.(Ray & Okamoto, 2003) Tan δ values in nanocomposite structures are influenced by the polymer matrix and the way the nanocomposite forms. Tan δ values were recorded at higher temperatures and expanding transitions in the nanostructures that were generated by modification with C14, C16, and C18 alkyl groups. Table 2 provides the glass transition temperature values determined from the peak maxima in the Tg and tan δ curves for both the copolymer and polymer/clay nanocomposites.

Thermal Analysis of Poly(3,4-Dihydro-2H-pyran-*co*-maleic anhydride-*co*-vinyl acetate) Terpolymer and its Nanocomposites

Thermal techniques were used to evaluate the thermal characterization of nanostructures made using terpolymers and three distinct alkyl ammonium salts. Figure 11 displays the temperature thermograms and mass loss percentages for the modified nanocomposites and

https://doi.org/10.1180/clm.2025.4 Published online by Cambridge University Press

terpolymers. Upon examining the poly(DHP-*co*-MA-*co*-VA) terpolymer thermogram shown in Figure 11-a, it can be observed that the terpolymer structure exhibits a two-step degradation, similar to the copolymer. Two degradation temperatures are observed: one at 280 °C and the other at 420 °C. The groups that are more readily removed from the terpolymer structure are those whose mass loss is 41.06% up to 300 °C. The mass loss in the copolymer thermogram is reported to be 34.85% in the first decay up to 300 °C and 44.05% in the terpolymer.

This variation might be the result of the terpolymer absorbing more hydrated components into its matrix and becoming more organically organized due to the vinyl acetate content. The degradation process in which species like CO_2 are extracted from the vinyl acetate groups and anhydride ring may be understood as the maximal degradation phase at 420 °C, which results in a mass loss of 45.7%. Again, the mass loss in the terpolymer (Figure 11-a) during the second phase of degradation is larger than that found in the copolymer. Based on a broad examination of Figure 11, the terpolymer structure exhibiting the maximum mass loss rate of 89.74% in mass loss-temperature thermograms up to 600 °C is identified. When the thermograms of nanocomposites generated with three different organo ammonium salts are investigated (Figure 11-b, c, and d), the overall breakdown stages are three steps, unlike terpolymer.

On thermograms, mass loss is noticed due to the elimination of H_2O crystal water between 100 and 180 °C, which is likewise lost in the bentonite structure. The stage where the largest mass loss is recorded is the first-line decay up to 200 °C. The mass loss of HDTMAB and TDTMAB-modified nanostructures up to 200 °C may be represented as 48.37% and 47.69%, respectively. On the other hand, the changed nanostructure with ODTMAB lost less mass than the other modified structures in this stage, and just 27.75% of it deteriorated. The substantial mass loss induced by lengthy alkyl chains in the first stage was not detected in the ODTMAB-modified nanocomposite.

This can be explained by the fact that the terpolymer and modified clay layers interact chemically more with ODTMAB than with TDTMAB in modified nanostructures. Between 200 and 360 °C, the modified nanocomposite structure with ODTMAB lost mass at a rate of 22.99%, identical to the terpolymer, whereas the modified nanostructures with HDTMAB

https://doi.org/10.1180/clm.2025.4 Published online by Cambridge University Press

and TDTMAB saw a mass loss of roughly 7%. 89.74% of the terpolymer, 80.72%, 74.35%, and 71.21% of the structures treated with ODTMAB sustained heat treatment up to 600 °C. HDTMAB, and DTMAB, respectively, were degraded. By incorporating 3 different inorganic-organic materials modified through 5% polymerization, nanocomposite structures with similar thermal stability were obtained. Thermal characterization revealed that the thermal stability of nanocomposites obtained using bentonite structures modified with organoammonium salts in a terpolymerization environment increases. Furthermore, the chain length of salts with long carbon chains used in modification plays a significant role in thermal stability. Table 2 presents the mass loss percentages of the terpolymer and nanocomposites, along with the glass transition temperatures obtained through 3 different methods. Glass transition temperatures were derived from the DTA (Figure 12) and DMA (Tan δ) curves, showing consistent trends across the methods. Notably, no significant difference in glass transition temperature (Tg) was observed between the terpolymer and its nanocomposites.

Table 2 shows the thermoanalytical data obtained by using DSC, DTA, and TGA thermal techniques. The glassy transition temperature was used comparatively from DTA and DSC analyses. Considering the C14-C18 chain lengths, the Tg values obtained from DTA and DSC are very highly compatible. The Tg values of the hybrid structures obtained as a result of the addition of inorganic material to the structures were found to be higher than copolymer (132.7 ^{o}C). The C16-C18 Tg values of the nanocomposites modified with HDTMAB and ODTMAB were found to be very similar to each other (140.56 ^{o}C and 140.78 ^{o}C). As a result of the characterization carried out by thermal methods, it is observed that the nanostructures obtained by using inorganic-organic modified structures in a copolymerization medium acquire thermal stability, and carbon chain lengths play an important role in this.

Dynamic Mechanical Analysis of Poly(3,4-Dihydro-2H-pyran-*co*-maleic anhydride-*co*-vinyl acetate) Terpolymer

Concerning temperature and constant frequency, the viscoelastic behavior of powdered copolymers and their nanocomposites (PCNs) was investigated using the DMA. To evaluate

https://doi.org/10.1180/clm.2025.4 Published online by Cambridge University Press

the homogeneous distribution of the organoclay structure in the polymer matrix and provide information on its distribution properties, DMA parameters are utilized. When examining the storage modulus (SM)-temperature (T) curve (Figure 13), the structure of the copolymer clay nanocomposite, which was made using the C18 alkyl group (Figure 13-a), exhibits the highest value of storage modulus.

High storage modulus (SM) values for the copolymer and PCN are suggested by the glassy zone that is present during the SM/T bending process up to 60 °C. With temperature increases (60–80 °C), the SM value of the sequential copolymer reduces rapidly. The changes in carbon chain length cause clays treated with C14, C16, and C18 to exhibit different patterns in their storage modulus values. Although our results at first suggested that elastic modulus would harmoniously increase with longer carbon chain lengths (Fig. 13), further investigation shows that, despite its shorter carbon chain length, C14's storage modulus has the highest value among PCNs over the whole temperature range. Similar observations were made about the glassy transition, and elastic areas' tendencies in their SMs. This shows that the layered silicate structure is spread throughout the polymer matrix.(Lan & Pinnavaia, 1994; Rzayev, 2010)

The temperature increases lead to the maximums at which Tg may be seen in the LM and Tan δ curves (Figures 14 and 15). The onset of "micro Brownian" movement between the molecular chains is indicated by the damping being low below Tg and increasing as the system gets closer to the Tg area.(Okamoto, 2009) This can be explained by the fact that not all segments unwind together, while the glassy segments contain more energy. When it comes to the rubbery region, it is believed that the segments in the solid state become liberated and give out excess energy. Micro-Brownian movement in a polymer chain can be expressed as the transition of one chain to diffusion by interacting with the other chain. The highest maximum damping is seen where the polymer chains contact each other under harmonic stress. In this situation, the loss modulus declines above Tg, and if it is around Tg, the segments start to gain movement and display minimal resistance to flowing.(Okamoto, 2009) In nanocomposite structures, Tan δ values are changed based on the creation of the nanocomposite and polymer matrix. Tan δ values were recorded at higher temperatures, indicating extended transitions in nanostructures modified with C14, C16, and C18 alkyl groups.(Patel *et al.*, 2006)

https://doi.org/10.1180/clm.2025.4 Published online by Cambridge University Press

The terpolymer shows a greater elastic modulus than the copolymer structure and the copolymer-clay nanocomposites, according to an analysis of the SM/T curves of the terpolymer and terpolymer-clay nanocomposites. The typical SM/T behavior is consistent with copolymer structures. SM is 700 GPa in the glassy zone (up to 60 °C) and is greater than the copolymer (~500 GPa). In contrast to nanostructures in the glassy transition zone (80–140 °C), there is a fast reduction in the terpolymer structure up to ~200 GPa. The copolymer structure is stable at approximately 100 GPa. This phenomenon might be understood by studying the interaction between three separate monomer groups, which engage in charge transfer complexes, resulting in nanostructures that demonstrate improved compatibility with shorter carbon chains due to their lower volume occupancy.(Ray & Okamoto, 2003; Kaplan *et al.*, 2012)

Table 3. Thermoanalytical results of Poly(DHP-*co*-MA-*co*-VA) and Poly(DHP-*co*-MA-*co*-VA)/organo-bentonite nanocomposites; % mass loss and Tg (^{0}C) values of terpolymer and polymer/clay nanocomposites at certain temperatures

Samples	**Glass Transition Temperatures Tg (°C)**			**Mass Loss (%)-Temperature(°C)**					
	DTA	**DSC**	**DMA**	**100**	**200**	**300**	**400**	**500**	**600**
Poly(DHP-*co*-MA-*co*-VA)	142	130	124	3.00	21.70	44.05	63.10	85.60	89.75
Poly(DHP-*co*-MA-*co*-VA)/ODTMAB-bentonite nanocomposite	146	123	149	0.15	27.75	50.75	61.85	78.00	80.70
Poly(DHP-*co*-MA-*co*-VA)/HDTMAB-bentonite nanocomposite	140	130	119	1.45	46.40	56.05	67.35	72.90	74.35
Poly(DHP-*co*-MA-*co*-	143	130	118	1.60	48.70	55.30	63.70	69.50	71.20

https://doi.org/10.1180/clm.2025.4 Published online by Cambridge University Press

VA)/)/TDTMAB-bentonite nanocomposite									

(poly(3,4-dihydro-2H-pyran-*co*-maleic anhydride-*co*-vinyl acetate); TDTMAB: tetradecyl (trimethyl) ammonium bromide; HDTMAB: hexadecyltrimethyl ammonium bromide; ODTMAB: octadecyltrimethyl ammonium bromide)

In the thermal investigation, maxima around 120 °C were detected in the loss modulus temperature (LM-T) and tanδ temperature (tan δ-T) curves. Preceding these peaks, sub-glass transition (Sub-Tg) events were identified, attributed to the mobility of side groups or aliphatic chains inside the polymer backbone. The Tg values of the terpolymer and nanostructures were obtained by utilizing the maximums of the Tan δ-T curves. Table 3 displays the Tg values obtained by DMA analysis. The large peaks found above the glass transition temperature range (140–180 °C) can be connected to two phenomena: physical cross-linking and pseudo-melting of functional groups inside the terpolymer. Physical cross-linking is most likely the result of interactions between functional groups such as carboxyl or hydroxyl groups. On the other hand, the pseudo-melting response reveals the softening or partial melting of these groups of functions when subjected to thermal stress. This reveals a complicated interplay of molecular interactions and heat effects inside the terpolymer architecture.

CONCLUSION

The current study utilized an *in-situ* solution polymerization method to synthesize poly(DHP-*alt*-MA) and poly(DHP-*co*-MA-*co*-VA) copolymers, along with their respective nanocomposites. These nanocomposites were created by modifying bentonite, which has a layered silicate structure, using three different alkyl ammonium salts: ODTMAB, HDTMAB, and TDTMAB, through ion exchange processes. After modification, the transformation of bentonite occurred from hydrophilic character to hydrophobic. Charge transfer complex reactions led to the formation of poly(DHP-*alt*-MA) copolymers, poly(DHP-*co*-MA-*co*-VA) terpolymers, containing electron acceptor-donor groups and nanocomposites incorporating clays modified with long alkyl chains of organoammonium salts.

Dynamic mechanical properties and thermal behaviors were investigated using DMA, DSC, DTA, and TGA. The evaluation of dynamic mechanical characteristics across modified bentonite configurations, including poly(DHP-*alt*-MA), poly(DHP-*co*-MA-*co*-VA), and the

https://doi.org/10.1180/clm.2025.4 Published online by Cambridge University Press

resulting polymer/clay nanocomposites, provided significant insights. Particularly noteworthy was the discovery that organoclay matrices, modified with both pristine bentonite and alkyl ammonium groups such as C14, C16, and C18, exhibited the highest mechanical strength among all bentonite derivatives. Furthermore, the organoclay treated with C18 ammonium salt showed strength values closest to those of bentonite. Upon examining the co- and terpolymer structures and their respective nanocomposites, it becomes evident that the terpolymer exhibits a higher elastic modulus compared to both the copolymer and the copolymer-clay and terpolymer-clay nanostructures. Thermal analysis results indicate that bentonite undergoes modification through ion exchange reactions with ODTMAB, HDTMAB, and TDTMAB, resulting in decreased thermal stability due to the addition of aliphatic long-chain structures to the modified forms. Thermograms of the copolymer/clay nanocomposites reveal a distinct three-step process, unlike the two-step process observed in the copolymer alone. However, there is no significant difference in the thermal stability among the copolymer, terpolymer, and their nanocomposites.

Conflict of Interest

The authors of the manuscript solemnly declare that no scientific and/or financial conflicts of interest exist with other people or institutions.

REFERENCES

Can, H.K., Doğan, A.L., Rzaev, Z.M., Uner, A.H. & Güner, A. (2005) Synthesis and antitumor activity of poly (3, 4-dihydro-2h-pyran-co-maleic anhydride-co-vinyl acetate). *Journal of applied polymer science*, **96**, 2352-2359.

Can, H.K., Sevim, H., Şahin, Ö. & Gürpınar, Ö.A. (2022) Experimental routes of cytotoxicity studies of nanocomposites based on the organo-bentonite clay and anhydride containing co-and terpolymers. *Polymer Bulletin*, **79**, 5549-5567.

Chan, M.-H., Lu, C.-N., Chung, Y.-L., Chang, Y.-C., Li, C.-H., Chen, C.-L., Wei, D.-H. & Hsiao, M. (2021) Magnetically guided theranostics: Montmorillonite-based iron/platinum nanoparticles for enhancing in situ mri contrast and hepatocellular carcinoma treatment. *Journal of nanobiotechnology*, **19**, 1-16.

Donaruma, L.G., Ottenbrite, R.M. & Vogl, O. (1980) *Anionic polymeric drugs*. Wiley.

https://doi.org/10.1180/clm.2025.4 Published online by Cambridge University Press

Gorshkova, M.Y. & Stotskaya, L.L. (1998) Micelle-like macromolecular systems for controlled release of daunomycin. *Polymers for Advanced Technologies*, **9**, 362-367.

Grim, R.E. & Guven, N. (2011) *Bentonites: Geology, mineralogy, properties and uses*. Elsevier.

Kaplan Can, H. & Şahin, Ö. (2015) Design, synthesis and characterization of 3, 4-dihydro-2h-pyran containing copolymer/clay nanocomposites. *Journal of Macromolecular Science, Part A*, **52**, 465-475.

Kaplan, S., Sadler, B., Little, K., Franz, C. & Orris, P. (2012) *Can sustainable hospitals help bend the health care cost curve?* Commonwealth Fund.

Kelley, E.G., Albert, J.N., Sullivan, M.O. & Epps III, T.H. (2013) Stimuli-responsive copolymer solution and surface assemblies for biomedical applications. *Chemical Society Reviews*, **42**, 7057-7071.

Lan, T. & Pinnavaia, T.J. (1994) Clay-reinforced epoxy nanocomposites. *Chemistry of materials*, **6**, 2216-2219.

Li, P.-R., Wei, J.-C., Chiu, Y.-F., Su, H.-L., Peng, F.-C. & Lin, J.-J. (2010) Evaluation on cytotoxicity and genotoxicity of the exfoliated silicate nanoclay. *ACS Applied Materials & Interfaces*, **2**, 1608-1613.

Liang, S., Zhang, M., Biesold, G.M., Choi, W., He, Y., Li, Z., Shen, D. & Lin, Z. (2021) Recent advances in synthesis, properties, and applications of metal halide perovskite nanocrystals/polymer nanocomposites. *Advanced Materials*, **33**, 2005888.

Marouf, R., Dali, N., Boudouara, N., Ouadjenia, F. & Zahaf, F. (2021) Study of adsorption properties of bentonite clay. Pp. *Montmorillonite clay*,IntechOpen.

Masindi, V. (2015) Remediation of acid mine drainage using magnesite and its bentonite clay composite.

Mir, M., un Nisha, I., Ahmed, N. & ur Rehman, A. (2025) Functionalized nanoclays in pharmaceutical industry. Pp. 145-176. *Functionalized nanoclays*,Elsevier.

Mobaraki, M., Karnik, S., Li, Y. & Mills, D.K. (2022) Therapeutic applications of halloysite. *Applied Sciences*, **12**, 87.

Modabberi, S., Namayandeh, A., López-Galindo, A., Viseras, C., Setti, M. & Ranjbaran, M. (2015) Characterization of iranian bentonites to be used as pharmaceutical materials. *Applied Clay Science*, **116**, 193-201.

https://doi.org/10.1180/clm.2025.4 Published online by Cambridge University Press

Mortimer, G.M., Jack, K.S., Musumeci, A.W., Martin, D.J. & Minchin, R.F. (2016) Stable non-covalent labeling of layered silicate nanoparticles for biological imaging. *Materials Science and Engineering: C*, **61**, 674-680.

Murray, H.H. (2006) *Applied clay mineralogy: Occurrences, processing and applications of kaolins, bentonites, palygorskitesepiolite, and common clays*. Elsevier.

Murugesan, S. & Scheibel, T. (2020) Copolymer/clay nanocomposites for biomedical applications. *Advanced Functional Materials*, **30**, 1908101.

Müller, K., Bugnicourt, E., Latorre, M., Jorda, M., Echegoyen Sanz, Y., Lagaron, J.M., Miesbauer, O., Bianchin, A., Hankin, S. & Bölz, U. (2017) Review on the processing and properties of polymer nanocomposites and nanocoatings and their applications in the packaging, automotive and solar energy fields. *Nanomaterials*, **7**, 74.

Nazir, M.S., Mohamad Kassim, M.H., Mohapatra, L., Gilani, M.A., Raza, M.R. & Majeed, K. (2016) Characteristic properties of nanoclays and characterization of nanoparticulates and nanocomposites. *Nanoclay reinforced polymer composites: Nanocomposites and bionanocomposites*, 35-55.

Okada, A. & Usuki, A. (2006) Twenty years of polymer-clay nanocomposites. *Macromolecular materials and Engineering*, **291**, 1449-1476.

Okamoto, M. (2009) Rheology in polymer/clay nanocomposites: Mesoscale structure development and soft glassy dynamics. Pp. 71-92. *Nano-and biocomposites*,CRC Press.

Okamoto, M. & Ray, S.S. (2004) Polymer/clay nanocomposites. *Encyclopedia of nanoscience and nanotechnology*, **8**, 791-843.

OTTENBRITE, R.M. (1982) The antitumor and antiviral effects of polycarboxylic acid polymers. Pp.,ACS Publications.

Patel, H.A., Somani, R.S., Bajaj, H.C. & Jasra, R.V. (2006) Nanoclays for polymer nanocomposites, paints, inks, greases and cosmetics formulations, drug delivery vehicle and waste water treatment. *Bulletin of Materials Science*, **29**, 133-145.

Ranjan, R., Verma, V., Dave, V. & Jha, P. (2025) Nanoclay-based drug delivery systems. Pp. 249-271. *Functionalized nanoclays*,Elsevier.

Rawtani, D. & Agrawal, Y. (2012) Multifarious applications of halloysite nanotubes: A review. *Rev. Adv. Mater. Sci*, **30**, 282-295.

https://doi.org/10.1180/clm.2025.4 Published online by Cambridge University Press

Ray, S.S. & Okamoto, M. (2003) Polymer/layered silicate nanocomposites: A review from preparation to processing. *Progress in Polymer Science*, **28**, 1539-1641.

Rzayev, Z.M. (2010) Polyolefin nanocomposites by reactive extrusion. *Advances in polyolefin nanocomposites*, 87-127.

Sabzevari, A.G. & Sabahi, H. Investigating the cytotoxicity of montmorillonite nanoparticles as a carrier for oral drug delivery systems. *Proceedings of the 2022 29th National and 7th International Iranian Conference on Biomedical Engineering (ICBME)*, 2022, IEEE, Pp. 256-260.

Sabzevari, A.G., Sabahi, H., Nikbakht, M., Azizi, M., Dianat-Moghadam, H. & Amoozgar, Z. (2024) Exploring the potential of montmorillonite as an antiproliferative nanoagent against mda-mb-231 and mcf-7 human breast cancer cells. *Cells*, **13**, 200.

Sánchez-Fernández, A., Peña-Parás, L., Vidaltamayo, R., Cué-Sampedro, R., Mendoza-Martínez, A., Zomosa-Signoret, V.C., Rivas-Estilla, A.M. & Riojas, P. (2014) Synthesization, characterization, and in vitro evaluation of cytotoxicity of biomaterials based on halloysite nanotubes. *Materials*, **7**, 7770-7780.

Singh, K., Kaur, S., Kaur, H. & Kaur, K. (2015) Multifaceted role of clay minerals in pharmaceuticals. *Future Science OA*, **1**, 1-9.

Srasra, E., Bergaya, F., Van Damme, H. & Ariguib, N. (1989) Surface properties of an activated bentonite—decolorisation of rape-seed oils. *Applied Clay Science*, **4**, 411-421.

Van Es, M. (2001) Polymer-clay nanocomposites. *Delft: PhD Thesis*.

Vergaro, V., Abdullayev, E., Lvov, Y.M., Zeitoun, A., Cingolani, R., Rinaldi, R. & Leporatti, S. (2010) Cytocompatibility and uptake of halloysite clay nanotubes. *Biomacromolecules*, **11**, 820-826.

Williams, L.B. & Haydel, S.E. (2010) Evaluation of the medicinal use of clay minerals as antibacterial agents. *International geology review*, **52**, 745-770.

Wirtu, S.F., Jule, L.T. & Nagaraj, N. (2025) Nanomaterials for biomedical applications: Drug delivery, biosensors, and tissue engineering. Pp. 125-150. *Exploring nanomaterial synthesis, characterization, and applications*,IGI Global.

Borah, D., Nath, H. & Saikia, H. (2022) Modification of bentonite clay & its applications: A review. *Reviews in Inorganic Chemistry*, **42**, 265-282.

https://doi.org/10.1180/clm.2025.4 Published online by Cambridge University Press

Wu, K., Feng, R., Jiao, Y. & Zhou, C. (2017) Effect of halloysite nanotubes on the structure and function of important multiple blood components. *Materials Science and Engineering: C*, **75**, 72-78.

Zhao, Y., Hu, J., Ke, Y., Long, Q., Mao, J., Li, H., Xiao, Z., Pan, K., Yuan, S. & Xue, J. (2024) Micro-interaction of montmorillonite-loaded nanoparticles with mucin promotes retention of betaxolol hydrochloride on the ocular surface and the tear film microenvironment. *Applied Clay Science*, **247**, 107198.

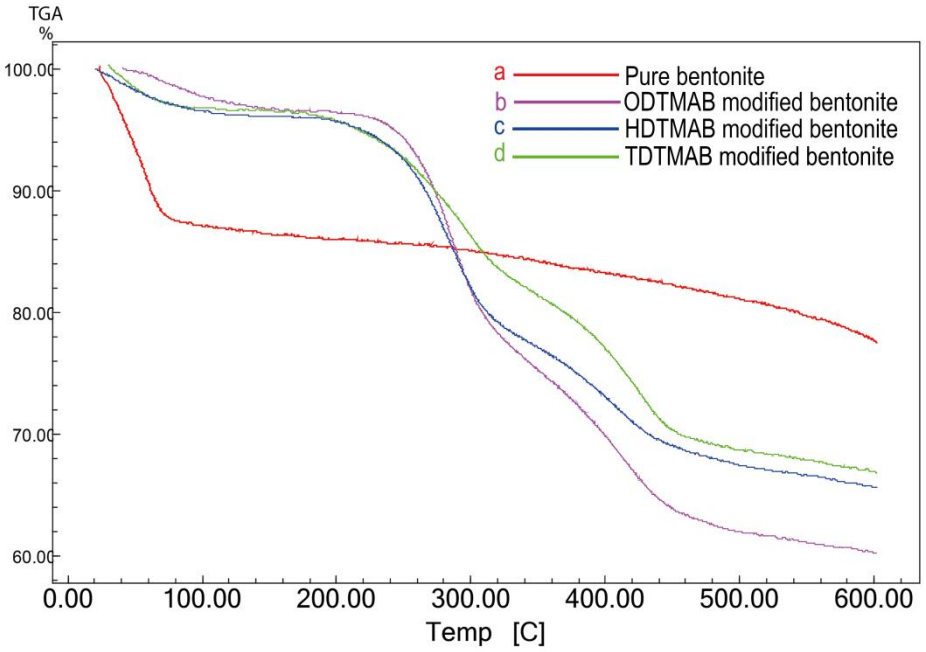

Figure 1. Termogravimetric analysis of bentonite (a), ODTMAB modified bentonite (b), HDTMAB modified bentonite (c), and TDTMAB modified bentonite (d) structures

https://doi.org/10.1180/clm.2025.4 Published online by Cambridge University Press

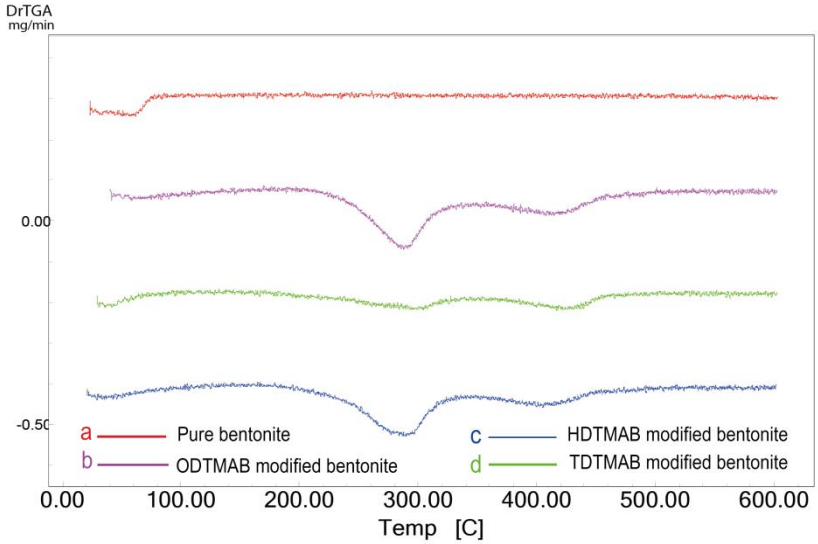

Figure 2. Differential thermogravimetric analysis of bentonite (a), ODTMAB modified bentonite (b), HDTMAB modified bentonite (c) and TDTMAB modified bentonite and (d) structures

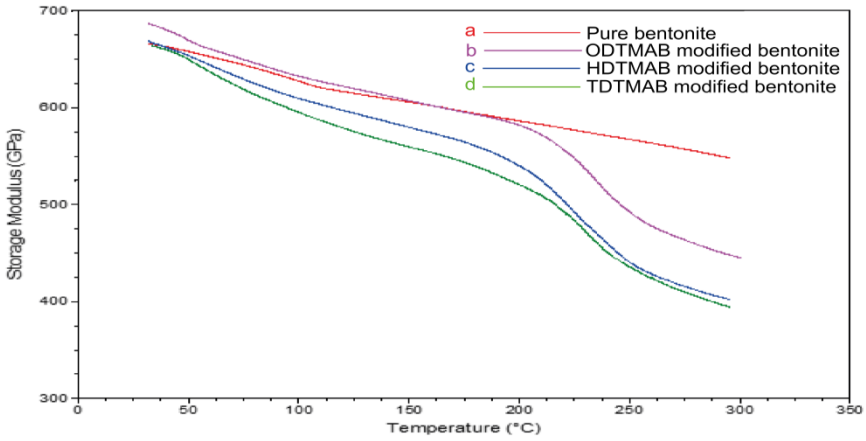

Figure 3. Storage modulus (SM)-temperature curves of bentonite (a), ODTMAB-modified bentonite (b), HDTMAB-modified bentonite (c) and TDTMAB-modified bentonite (d) structures

https://doi.org/10.1180/clm.2025.4 Published online by Cambridge University Press

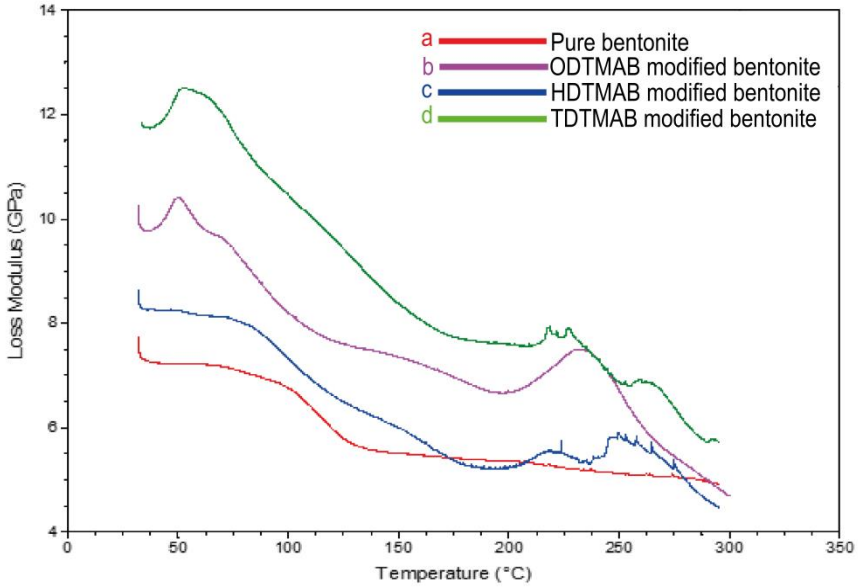

Figure 4. Loss modulus (LM)-temperature curves of bentonite (a), ODTMAB modified bentonite (b), HDTMAB modified bentonite (c), and TDTMAB modified bentonite (d) structures

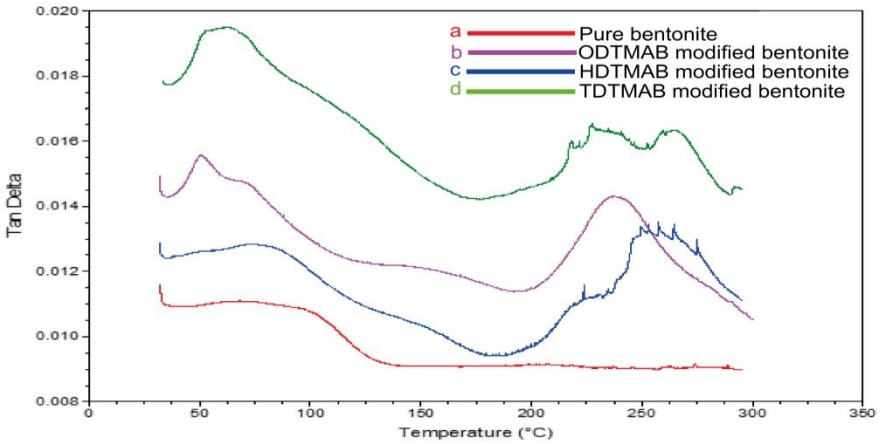

Figure 5. Tan δ-temperature curves of bentonite (a), ODTMAB modified bentonite (b), HDTMAB modified bentonite (c), and TDTMAB modified bentonite (d) structures

https://doi.org/10.1180/clm.2025.4 Published online by Cambridge University Press

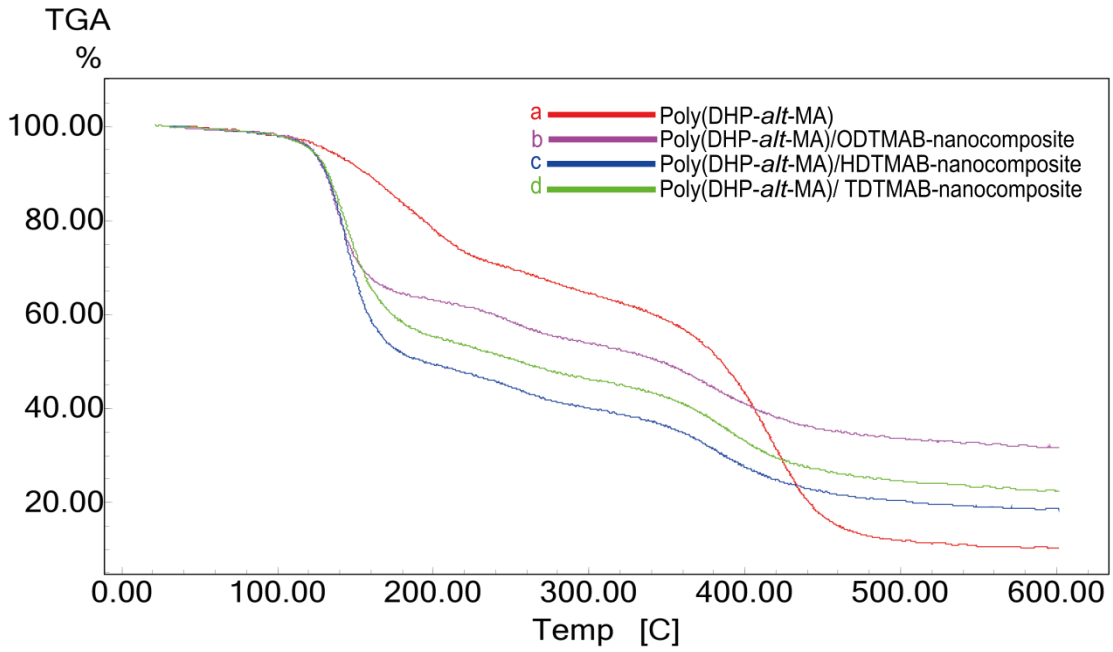

Figure 6. Thermogravimetrik analysis of poly (DHP-*alt*-MA) and organo-clay polymer nanocomposites

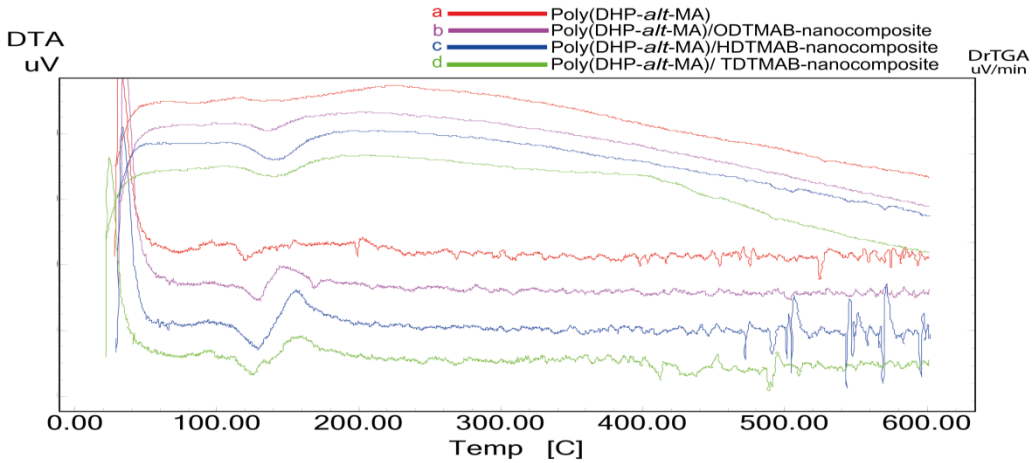

Figure 7. Differential thermal analysis (DTA) and Derivative Differential Thermal Analysis (DrDTA)/temperature plots of poly (DHP-*alt*-MA) and organo-clay copolymer nanocomposites

https://doi.org/10.1180/clm.2025.4 Published online by Cambridge University Press

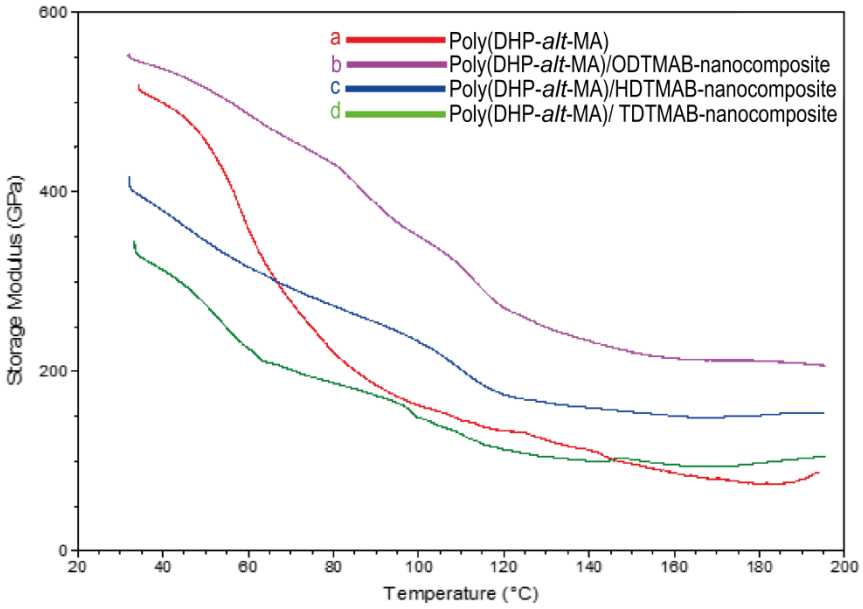

Figure 8. Storage modulus (SM)-temperature curves of copolymer and organo-clay copolymer nanocomposites: (a) poly(DHP-*alt*-MA), (b) poly(DHP-*alt*-MA)/ODTMAB-bentonite nanocomposite, (c) poly(DHP-*alt*--MA)/HDTMAB-bentonite nanocomposite, (d) poly(DHP-*alt*-MA)/TDTMAB-bentonite nanocomposite

https://doi.org/10.1180/clm.2025.4 Published online by Cambridge University Press

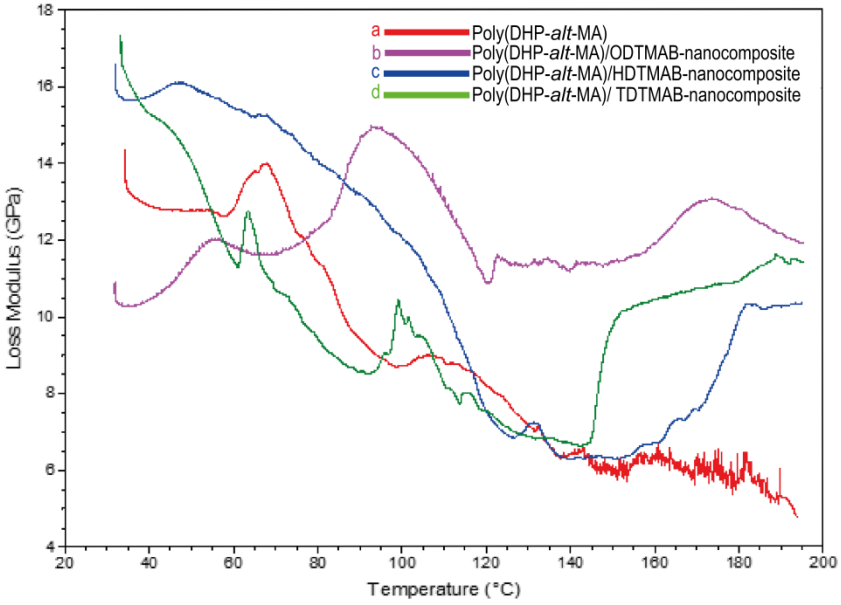

Figure 9. Loss modulus (LM)-temperature curves of copolymer and organo-clay copolymer nanocomposites: (a) poly(DHP-*alt*-MA), (b) poly(DHP-*alt*-MA)/ODTMAB-bentonite nanocomposite, (c) poly(DHP-*alt*-MA)/HDTMAB-bentonite nanocomposite, (d) poly(DHP-*alt*-MA)/TDTMAB-bentonite nanocomposite

https://doi.org/10.1180/clm.2025.4 Published online by Cambridge University Press

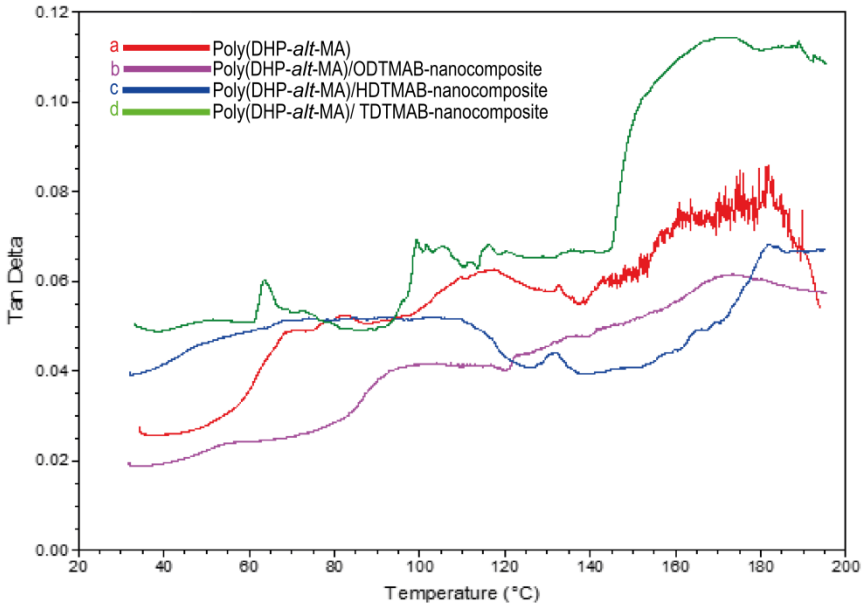

Figure 10. Tan δ-temperature curves of copolymer and organo-clay copolymer nanocomposites: (a) poly(DHP-*alt*-MA), (b) poly(DHP-*alt*-MA)/ODTMAB-bentonite nanocomposite, (c) poly(DHP-*alt*-MA)/HDTMAB-bentonite nanocomposite, (d) poly(DHP-*alt*-MA)/TDTMAB-bentonite nanocomposite

https://doi.org/10.1180/clm.2025.4 Published online by Cambridge University Press

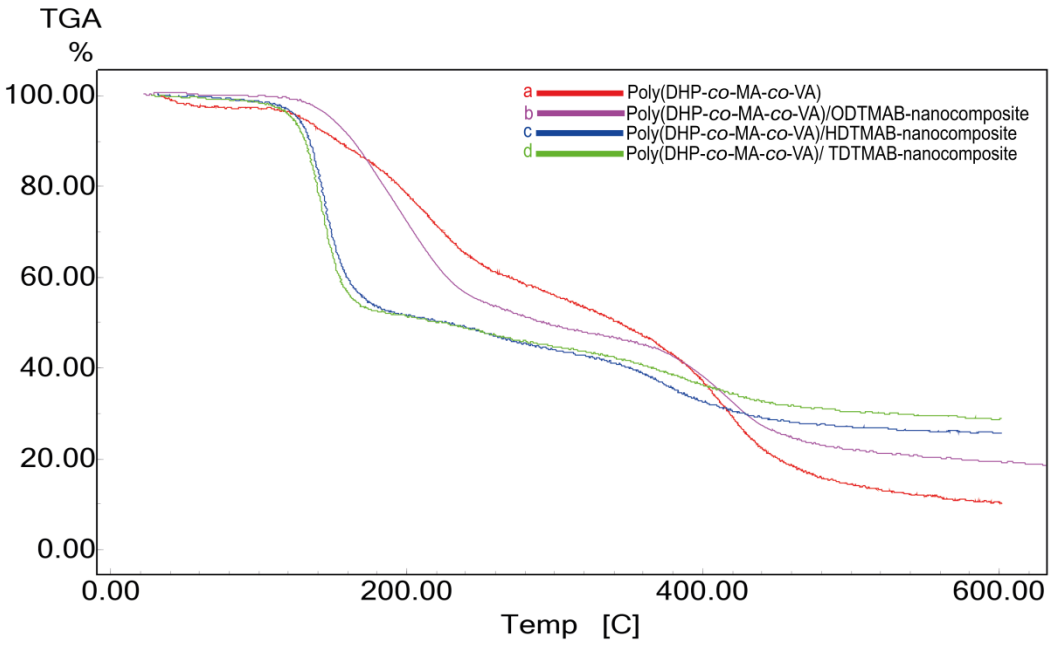

Figure 11. TGA/temperature diagrams of terpolymer and organo-clay terpolymer nanocomposites

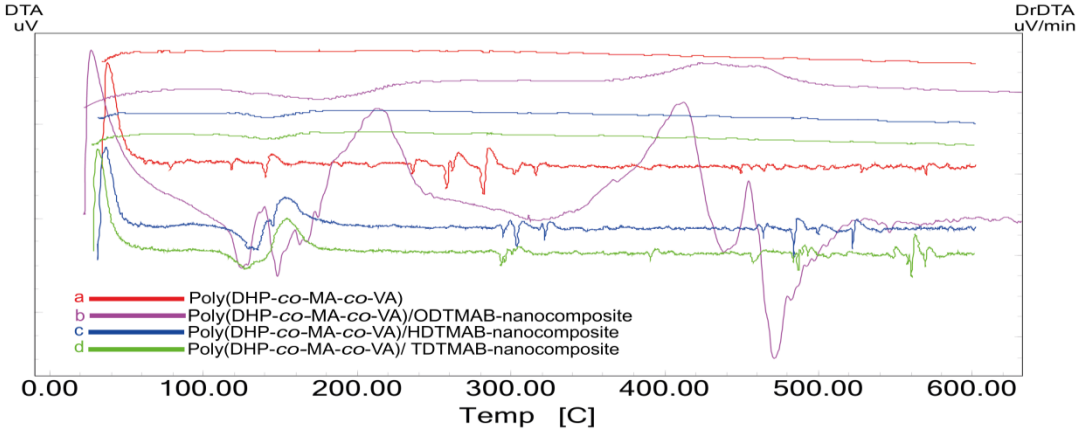

Figure 12. Differential Thermal Analysis (DTA) and Derivative Differential Thermal Analysis (DrDTA)/temperature plots of terpolymer and organo-clay terpolymer nanocomposites

https://doi.org/10.1180/clm.2025.4 Published online by Cambridge University Press

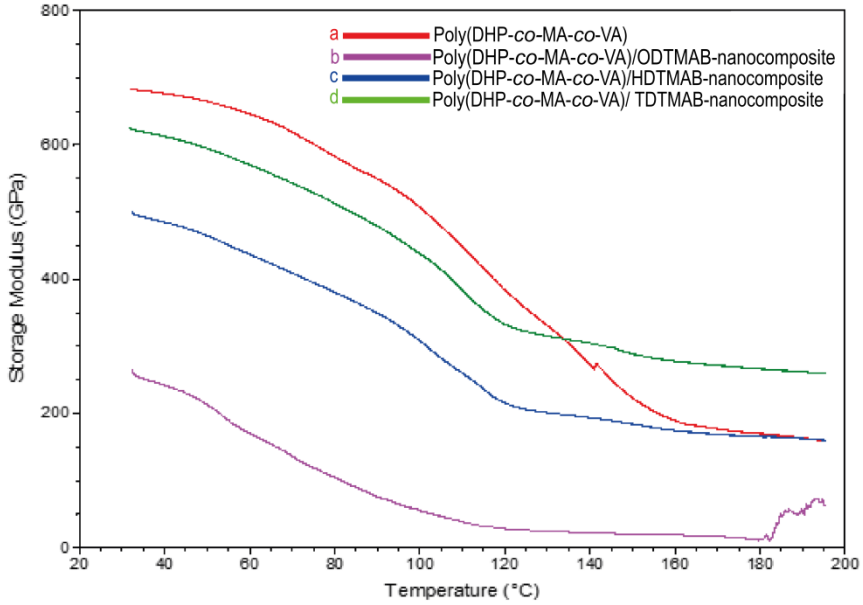

Figure 13. Storage modulus (SM)-temperature diagrams of terpolymer and organo-clay terpolymer nanocomposites: (a) poly(DHP-*co*-MA-*co*-VA), (b) poly(DHP-*co*-MA-*co*-VA)/ODTMAB-bentonite nanocomposite, (c) poly(DHP-*co*-MA-*co*-VA)/HDTMAB-bentonite nanocomposite, (d) poly(DHP-*co*-MA-*co*-VA)/TDTMAB-bentonite nanocomposite

https://doi.org/10.1180/clm.2025.4 Published online by Cambridge University Press

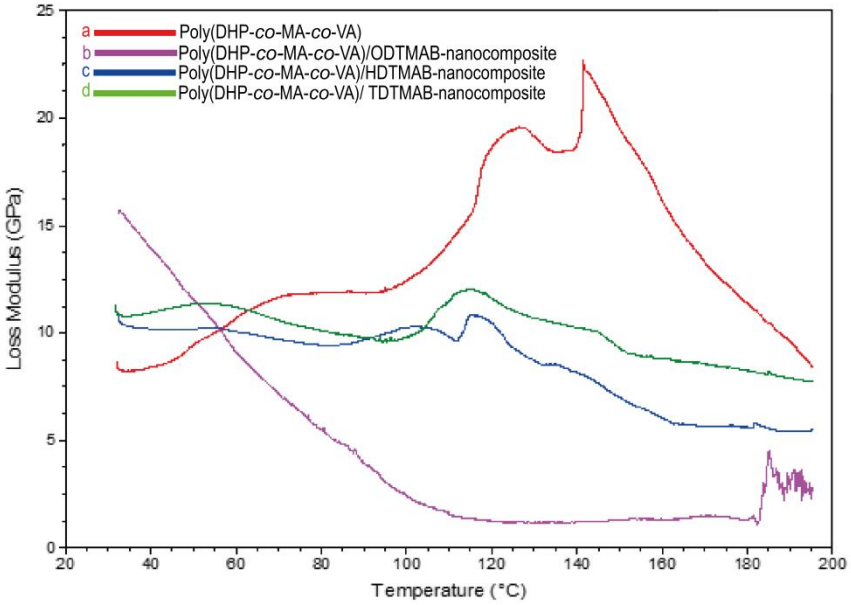

Figure 14. Loss modulus (LM)-temperature diagrams of terpolymer and organo-clay terpolymer nanocomposites: (a) poly(DHP-*co*-MA-*co*-VA), (b) poly(DHP-*co*-MA-*co*-VA)/ODTMAB-bentonite nanocomposite, (c) poly(DHP-*co*-MA-*co*-VA)/HDTMAB-bentonite nanocomposite, (d) poly(DHP-*co*-MA-*co*-VA)/TDTMAB-bentonite nanocomposite

https://doi.org/10.1180/clm.2025.4 Published online by Cambridge University Press

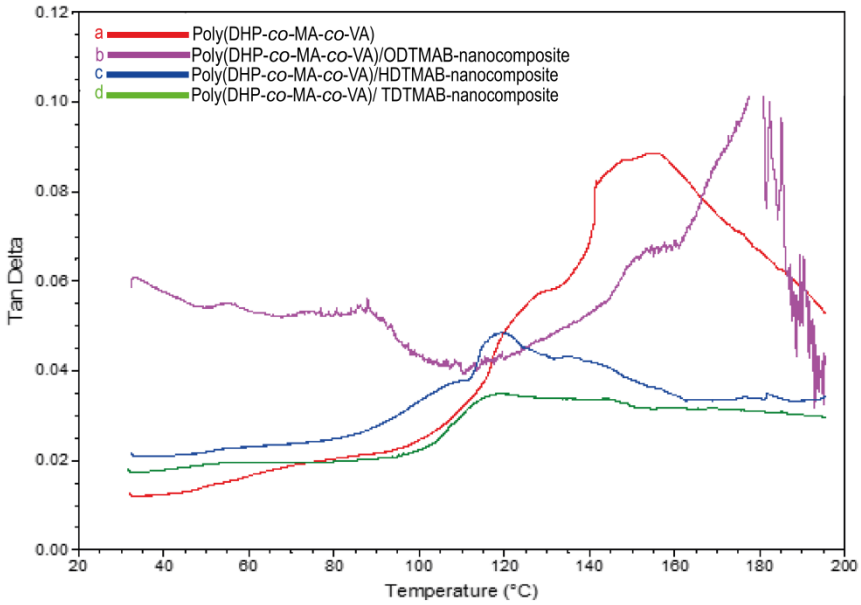

Figure 15. Tan δ-temperature diagrams of terpolymer and organo-clay terpolymer nanocomposites: (a) poly(DHP-*co*-MA-*co*-VA), (b) poly(DHP-*co*-MA-*co*-VA)/ODTMAB-bentonite nanocomposite, (c) poly(DHP-*co*-MA-*co*-VA)/HDTMAB-bentonite nanocomposite, (d) poly(DHP-*co*-MA-*co*-VA)/TDTMAB-bentonite nanocomposite

Declaration of Interest Statement

The authors of the manuscript solemnly declare that no scientific and/or financial conflicts of interest, exists with other people or institutions.

https://doi.org/10.1180/clm.2025.4 Published online by Cambridge University Press